Chemical Science

ROYAL SOCIETY OF CHEMISTRY

EDGE ARTICLE

View Article Online
View Journal | View Issue

Cite this: *Chem. Sci.*, 2023, **14**, 2616

All publication charges for this article have been paid for by the Royal Society of Chemistry

Received 14th October 2022
Accepted 5th February 2023

DOI: 10.1039/d2sc05747f

rsc.li/chemical-science

Confinement effect on hydrolysis in small lipid vesicles†

Ben Woods,[a] Katherine C. Thompson,[a] Nicolas Szita,[b] Shu Chen,[a] Lilia Milanesi[c] and Salvador Tomas *[ac]

In living organisms most chemical reactions take place within the confines of lipid-membrane bound compartments, while confinement within the bounds of a lipid membrane is thought to be a key step in abiogenesis. In previous work we demonstrated that confinement in the aqueous cavity of a lipid vesicle affords protection against hydrolysis, a phenomenon that we term here confinement effect (C_e) and that we attributed to the interaction with the lipid membrane. Here, we show that both the size and the shape of the cavity of the vesicle modulate the C_e. We link this observation to the packing of the lipid following changes in membrane curvature, and formulate a mathematical model that relates the C_e to the radius of a spherical vesicle and the packing parameter of the lipids. These results suggest that the shape of the compartment where a molecule is located plays a major role in controlling the chemical reactivity of non-enzymatic reactions. Moreover, the mathematical treatment we propose offers a useful tool for the design of vesicles with predictable reaction rates of the confined molecules, *e.g.*, drug delivery vesicles with confined prodrugs. The results also show that a crude form of signal transduction, devoid of complex biological machinery, can be achieved by any external stimuli that drastically changes the structure of the membrane, like the osmotic shocks used in the present work.

Introduction

Life on Earth is intimately linked to water. Chemical reactions involving water molecules play a central role in building complex molecules[1] as well as in storage and release of energy by means of condensation and hydrolysis reactions. Life requires therefore that a balance is struck between these opposite chemical processes.[2] In the bulk of a water solution, hydrolysis reactions are spontaneous, while condensation reactions are not. In water, any complex biomolecule, such as a protein or nucleic acid, would eventually hydrolyse, yielding amino acids and nucleotides. In living organisms, this problem is solved by coupling condensation with other reactions that provide the energy necessary to render the whole process spontaneous.[3,4] An archetypical condensation reaction in biochemistry is the formation of a peptide bond. The direct route, the reaction of the amine with the acid, is both non-spontaneous and has a large activation energy. A way around this issue is to transform the acid into a reactive species that will then react with the amine before it hydrolyses.[5] The resulting peptide bonds are thermodynamically unstable but inert in water, enabling the formation of large proteins. It is therefore critical that the reactive species is protected long enough so that the appropriate amine group reacts with it before hydrolysis.

In living cells, the suppression of hydrolysis is achieved by shielding the activated molecule from water within the pocket of the appropriate enzyme complex. But any other mechanism by which the activity of water is reduced would also result in the suppression of hydrolysis. In the context of abiogenesis this could have been accomplished simply by evaporation,[6,7] or by the inclusion of the activated molecule within the hydrophobic core of lipid membranes or micelles.[8–10] Trapping a molecule within the aqueous cavity of a lipid vesicle may also protect it from hydrolysis.[11,12] Such a "confinement effect" on hydrolysis may have played a significant role in shaping the chemical evolution of molecules trapped within protocells during abiogenesis.

In our previous work we carried out the detailed study of the hydrolysis of an activated ester. The protection against hydrolysis, *via* confinement in lipid vesicles, is attributed to the binding of the confined ester with the inner part of the lipid membrane.[12] It follows that this confinement effect should be proportional to the apparent lipid concentration within the cavity which, for spherical vesicles, is inversely proportional to the vesicle radius.

[a]*Department of Biological Sciences and Institute of Structural and Molecular Biology, Birkbeck, University of London, Malet Street, London WC1E 7HX, UK*

[b]*Department of Biochemical Engineering, University College London, Bernard Katz Building, Gordon Street, London WC1H 0AH, UK*

[c]*Department of Chemistry, University of the Balearic Islands, Ctra. de Valldemossa, Km 7.5, 07122 Palma de Mallorca, Spain. E-mail: salvador.tomas@uib.es*

† Electronic supplementary information (ESI) available: Detailed experimental procedures, derivation of the mathematical models, EM images and supplementary spectroscopic data. See DOI: https://doi.org/10.1039/d2sc05747f

In the present work, we set out to test this hypothesis while also exploring ways in which to exploit the confinement effect to modulate hydrolytic processes. We analyzed the hydrolysis of an activated ester in spherical vesicles of different sizes and in vesicles whose volume is drastically reduced by means of an osmotic shock.[13] While the latter does lead to a clear suppression of hydrolysis, consistent with the large increase in apparent lipid concentration, the picture offered by experiments on spherical vesicles is more complex. In these, the confinement effect (*i.e.*, the protection factor against hydrolysis) increases as the vesicle size decreases, down to a critical vesicle radius (about 50 nm). Further decrease of the vesicle radius leads to a downward trend in the confinement effect. In other words, from a critical size downwards the rate of hydrolysis increases.

We attribute these changes to variations in membrane binding of the ester that would depend on its curvature. Our results have allowed us to produce a model of binding affinity as a function of concave membrane curvature. The observation is consistent with studies that show that membrane curvature is a key factor in the regulation of the binding of membrane proteins and peptides.[14–18] While the effect of convex curvature in membrane binding has been rigorously characterized,[14–18] to the best of our knowledge the quantification (and modelling) of the binding to concave membranes has not been reported in the literature.

Overall, this work shows that the chemistry in lipid-bound compartments can be modulated by changing both the size and the shape of the compartment. Such regulation may play a role within living organisms, where compartments of different shapes are tasked to fulfil different roles. We also expand the toolbox for the design of efficient protocells as models of abiogenesis,[19–22] nanoreactors[23–25] and for the design of functional, biomimetic constructs for drug delivery and biosensing.[26–30]

Results and discussion

As previously shown,[12] amino acid derivative ester **1P** (Fig. 1(a)) features the chromophore pyranine and has a hydrolysis half-life of 8 hours in aqueous buffer at pH 7.2, making it ideally suited to be used as a probe to study hydrolysis in lipid vesicles. When confined within the cavity of vesicles of 100 nm radius, the half-life of hydrolysis of this probe is increased up to 200 hours. We define the experimental confinement effect on hydrolysis, C_e, as a protection factor against hydrolysis, that is:

$$C_e = \frac{k_b}{k} \quad (1)$$

where k_b is the rate constant of hydrolysis of the probe **1P** in the bulk solution and k the observed rate constant of hydrolysis of lipid vesicle-confined **1P** (Fig. 1(a) and (c)). The C_e for probe **1P** in a vesicle of 100 nm radius is therefore 25. **1P** has a moderate affinity for the membrane characterized by a membrane–probe dissociation constant K_d of 0.7 mM (Fig. 1(c)).[12] From the reference point of a membrane impermeable molecule, such as **1P**, the concentration of the lipids to which it is exposed is given by the ratio of the number of molecule of lipids in the inner leaflet of the membrane over the volume of the vesicle. In other words, the apparent concentration of lipid in the cavity, $[L]_c$, is proportional to the surface over volume ratio of the cavity. Therefore, for spherical vesicles it can be shown that $[L]_c$ is inversely proportional to the radius of the vesicles, r, according to eqn (2) (see the ESI,† Section 2.5, for detailed derivation):

$$[L]_c = \frac{3}{n_A a_m r} \quad (2)$$

where n_A is Avogadro's number and a_m the area per lipid molecule. The confinement leads to very large lipid concentrations for vesicles in the sub-micron size range. For example, for vesicles with 100 nm radius, with a membrane composed of

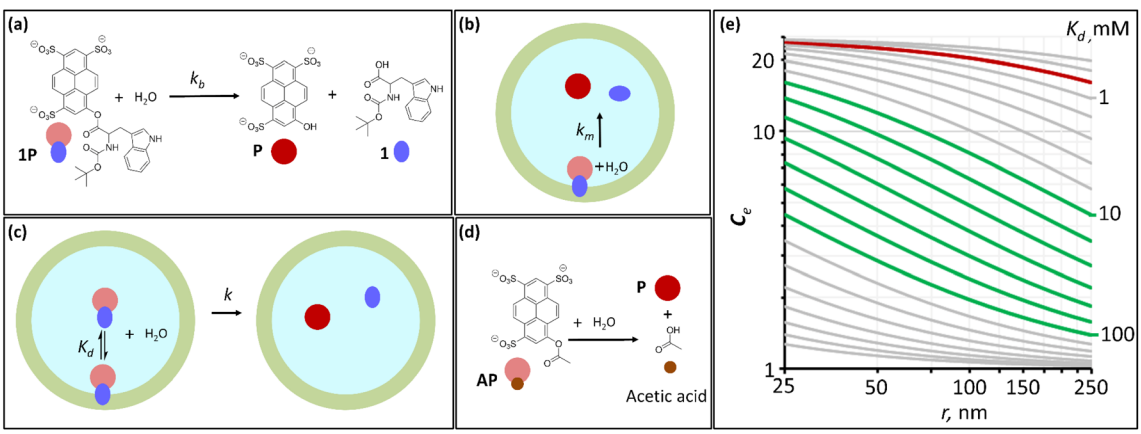

Fig. 1 Hydrolysis probes and the confinement effect on hydrolysis. (a) Reaction scheme of the hydrolysis of **1P**, together with the corresponding cartoon representations. (b) Cartoon representations of the hydrolysis of membrane-bound **1P** confined in a lipid vesicle. (c) Cartoon representation of the process of dissociation of membrane bound, confined **1P** and its hydrolysis. (d) Reaction scheme of the hydrolysis of **AP**, together with the corresponding cartoon representations. (e) Simulated changes in the confinement effect, C_e, with the lipid vesicle radius for hydrolysis probes with different affinities for the membrane, characterized by the dissociation constant K_d. The red trace represents the simulated changes in C_e for **1P** ($K_d = 0.7$ mM). The green traces represent the simulations for optimal values of K_d, where the dynamic range in C_e is the largest for LUV–SUV vesicle sizes (250–25 nm radius).

DOPC, the concentration of lipids in the cavity is 170 mM. Given the K_d of 0.7 mM of **1P** for the membrane, **1P** will be largely bound to the membrane when confined within vesicles in this size range. The confinement effect C_e is therefore readily attributed to the binding of the probe to the membrane, where it is protected against hydrolysis on account of the lower water activity at the membrane–water interface. It follows that for any molecule that can undergo hydrolysis, it is possible to build a theoretical model for the confinement effect as a function of the radius of the vesicle, the rate constants of hydrolysis in bulk water (k_b), the rate constant of hydrolysis when bound to the membrane (k_m) and the molecule–membrane dissociation constant K_d (Fig. 1(a)–(c)). Let's call the membrane bound fraction of the molecule α. The rate constant of hydrolysis of confined molecules can be written as:

$$k = (1 - \alpha)k_b + \alpha k_m \quad (3)$$

The bound fraction α depends in turn on the affinity of the probe for the lipid, characterized by the lipid–probe dissociation constant K_d. Typically, for vesicles with diameters below 1 μm, the concentration of lipid in the cavity is much larger than that of the confined probe. Under these conditions, α can be written as:

$$\alpha = \frac{[L]_c}{K_d + [L]_c} \quad (4)$$

Combining eqn (1)–(4) (see the ESI,† Section 3.1, for detailed derivation) we have:

$$C_e = \frac{3k_b + n_A A_L k_b K_d r}{3k_m + n_A A_L k_b K_d r} \quad (5)$$

Eqn (5) recapitulates the theoretical model of the confinement effect on hydrolysis and shows that, for confined molecules, C_e tends to a maximum value when r tends to 0, a hypothetical scenario (in practice, lipid bilayers do not form below a critical size) in which all the probe will find itself bound to the membrane, in the absence of an aqueous cavity. On the other hand, C_e tends to 1 for large vesicle radii. In these cases, the apparent concentration of the lipids will be, eventually, low enough as to the binding of the probe not having a measurable effect on its hydrolysis. Eqn (5) predicts in simple terms the reactivity of hydrolysable molecules inside spherical vesicles. It offers therefore a useful tool for the study of biochemistry in cellular confined spaces, nanoreactors and for the design of delivery vehicles, where gaining an optimal control of the rate of release of the contents is highly desirable.

Testing the validity of eqn (5) requires that we measure C_e experimentally with vesicles of different radius. Taking into account the 0.7 mM value of K_d, the C_e for **1P** is near its maximum value of 25 for vesicles of 100 nm diameter. Simulations using eqn (5) show that it would experience little increase in its value for the range of vesicle size typical of LUV and SUV (*i.e.*, Large and Small Unilamellar Vesicles, with radius ranging from 250 to 25 nm) (Fig. 1(e), red trace), the target size of interest in nanoreactors, drug delivery vehicles and transport vesicles in living cells. Obtaining a measurable range of C_e requires therefore that we use a hydrolysis probe with an affinity for the membrane much lower than **1P**. For a molecule with similar chemical reactivity to **1P** (*i.e.*, similar k_b and k_m), the optimal dynamic range for our studies requires that it has a dissociation constant for the membrane, K_d, between 10 and 100 mM according to the simulations based on eqn (5) (Fig. 1(e)). Hydrolysis probe **AP**, which contains the same chemical functionality but lacks the hydrophobic moiety of the tryptophan derivative in **1P** and therefore is expected to have lower affinity for lipids, was chosen as an ideal candidate to undertake these studies (Fig. 1(d)).

AP was synthesized and purified according to literature methods.[25] The lipid vesicles were composed of DOPC containing different molar percentages of the cationic lipid DODAB (0, 2.5, 5 and 10%) to modulate the affinity of the negatively charged probe **AP** for the membrane.

In all our experiments (except when specified in the osmotic shock experiments) we used as solvent a solution of NaCl 2 M, in sodium phosphate buffer 100 mM, pH 7.2. (see the ESI,† Section 1, for further details on sample preparation). We first attempted to determine the membrane–**AP** dissociation constant by means of a UV spectroscopy titration method. As the concentration of vesicles is increased, the UV spectrum of **AP** shows changes consistent with membrane binding for all of the four membrane compositions tested (ESI Fig. S1†). The low affinity of **AP** for the membrane makes it however challenging to obtain a reliable value of K_d. Only for vesicles with 10% DODAB in the membrane the extent of binding is large enough to allow estimating a value of 30 mM K_d from the UV data (see the ESI,† Section 2.1, for details). These experiments confirm that the affinity of **AP** for the vesicle is within the 10 to 100 mM range necessary to obtain an adequate window for the confinement effect in our experiments (Fig. 1(e)).

The release of pyranine allows us to monitor the extent of hydrolysis of **AP** by recording changes in its UV spectrum at different time intervals.[12] These changes fit well into a 1st order kinetic process from which a rate constant of hydrolysis of **AP** in the bulk solvent of 0.094 h^{-1} ($t_{1/2}$ of 7.4 h) is determined, which is the same value, within error, obtained for **1P**.[12] The presence of lipid vesicles up to a concentration of 5 mM did not have a measurable effect on the rate of hydrolysis of **AP**, for any of the membrane compositions tested. This result is consistent with the low binding affinity of **AP** for the membrane.

Initial confinement experiments were aimed at obtaining the rate of hydrolysis under extreme confinement conditions. To that aim, vesicles containing confined **AP** were produced with an average radius of 110 nm (as measured by DLS) and were shrunk by means of an osmotic shock (see the ESI,† Section 1, for experimental details). Upon hypertonic osmotic shock, the membrane of spherical vesicles tends to fold into itself, giving rise to stomatocyte-like structures.[13] During this process, the original spherical cavity becomes a spherical shell between the inner and outer membrane of the stomatocyte (ESI Fig. S5†). In our experiments, the osmotic shock resulted from a 20-fold

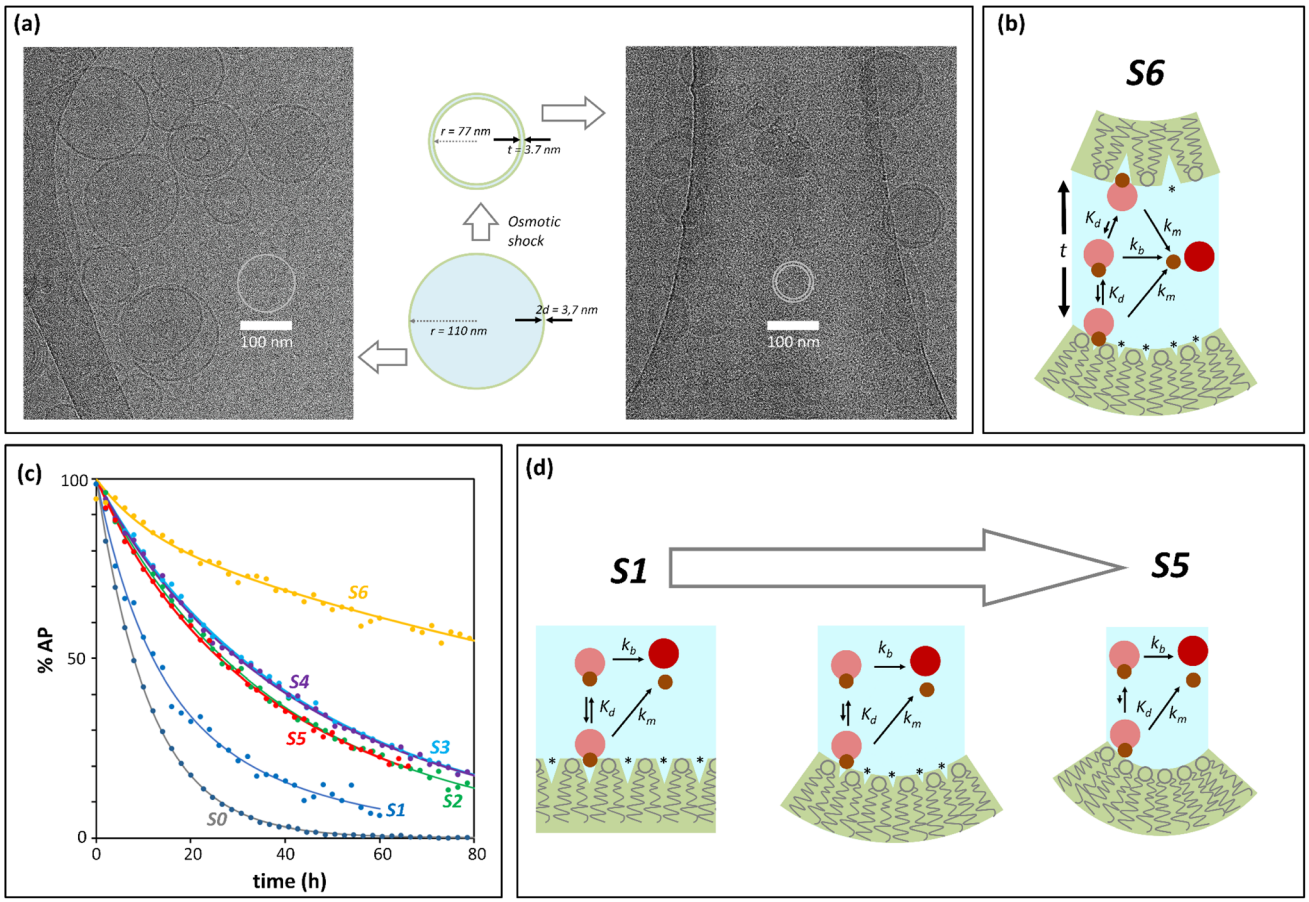

Fig. 2 Confinement effect *vs.* curvature. (a) Cryo-EM images. The central cartoon represents the predicted structural changes of a vesicle upon application of the osmotic shock, shown to scale. 2*d* is the thickness of the membrane and *t* that of the intermembrane water layer after osmotic shock (see the ESI,† Section 2.8, for calculation details). The left side panel is a Cryo-EM image of vesicles before osmotic shock is applied. The right side panel is the Cryo-EM image of vesicles that have undergone osmotic shock. (b) Cartoon representation of the membrane-binding and hydrolysis of **AP** confined in the cavity of a vesicle that has undergone osmotic shock. (*) represents membrane defects. The label S6 is used for this type of experiment in panel (c) and Table 1. (c) Percentage of unreacted **AP** with time after hydrolysis, derived from UV data (solid dots) and their fitting to the corresponding kinetic process (solid lines). The labels are color-coded and refer to: S0, non-confined **AP**. S1 to S5, **AP** confined in vesicles of decreasing radius (see Table 1), S6, osmotically shrunk vesicles. (d) Cartoon representation of the possible effects resulting from an increase of curvature and decrease in vesicle radius (from S0 to S5): reduction of lipid packing defects (labelled with *), of **AP** binding and hydrolysis.

gradient in osmotic pressure between the bulk and the vesicle cavity. Our calculations show that a 20 fold-decrease in the volume of the cavity is required in order to re-equilibrate the pressure. Therefore, provided that the membrane of the vesicles maintains its integrity and the process does not involve leakage of the content, the spherical shell of the resulting stomatocyte will contain 1/20 of the volume of the spherical cavity in the original vesicle (see the ESI,† Section 2.8, for calculation details).[31,32] Membranes composed of DOPC are, at room temperature, in the liquid disordered state, allowing for dramatic shape changes without breakage. Fluorescence quenching experiments show that the shock did not lead to release of confined **AP**, confirming that the integrity of the membrane was maintained (ESI Fig. S3†). From geometric considerations, it is possible to estimate the approximate structure of a stomatocyte arising from the 20-fold volume reduction of a spherical vesicle. Thus, a vesicle with a 110 nm radius will become a stomatocyte with an overall radius of 77 nm and with an inter-membrane water layer of about 3.7 nm thickness (Fig. 2(a), see the ESI,† Section 2.8, for calculation details). This is about the same thickness of a DOPC membrane. The implication is that these stomatocytes would resemble double-lamella vesicles. Cryo-EM imaging of vesicle samples is consistent with this scenario and the calculated measurements for the double-lamella, stomatocyte structures (Fig. 2(a)). Thus, for samples of vesicles before osmotic shock, unilamellar vesicles are the dominant structures seen. For samples subjected to osmotic shock, double-lamella vesicles are dominant (Fig. 2(a), ESI Fig. S5 and EM images†). The lipid concentration in the inter-membrane cavity of these vesicles can be estimated from the expected 20-fold volume reduction. Therefore, vesicles of 110 nm radius, with $[L]_c$ of 62 mM according to eqn (1), will end up with an $[L]_c$ of around 1230 mM when osmotically shrunk.

Table 1 Hydrolysis rate constants and half-lives, and the corresponding confinement effects[a]

		0% DODAB			2.5% DODAB			5% DODAB			10% DODAB		
Sample	Vesicle radius	k	$t_{1/2}$	C_e	k	$t_{1/2}$	C_e	k	$t_{1/2}$	C_e	k	$t_{1/2}$	C_e
S0	[b]	0.094	7.4	1	0.094	7.4	1	0.094	7.4	1	0.094	7.4	1
S1	150	0.050	14	1.9	0.047	15	2.0	0.042	16	2.2	0.029	24	3.3
S2	110	0.032	22	3.0	0.035	20	2.7	0.036	20	2.6	0.022	31	4.2
S3	75	0.028	25	3.4	0.029	24	3.2	0.034	21	2.8	0.019	36	4.9
S4	40	0.031	22	3.0	0.031	22	3.0	0.030	23	3.2	0.019	36	4.9
S5	30	0.031	22	3.0	0.031	22	3.0	0.030	23	3.1	0.020	34	4.6
S6	[c]	0.0052	132	18	0.0046	150	20	0.0039	179	24	0.0058	120	16

[a] Values of rate constant in h^{-1} and $t_{1/2}$ in h. The error in the measure is 20%, estimated as twice the standard deviation. [b] Hydrolysis in the bulk buffer (not confined). [c] Hydrolysis of **AP** confined in vesicles of 110 nm radius subjected to osmotic shock.

At this concentration of lipids, confined **AP**, with a K_d in the region of 30 mM, can be assumed fully bound to the membrane and the rate constant of hydrolysis obtained from these experiments as the intrinsic rate constant of membrane-bound probe, k_m (Fig. 2(b) and (c), Table 1). The value of the rate constant was similar in all compositions tested, with no discernible trend with the percentage of DODAB present in the membrane (Table 1). The average k_m calculated is 00 049 h^{-1} and the corresponding half-life is 142 hours. The maximum confinement effect C_e for **AP** is therefore 19.2. While somewhat smaller, this value is similar to that observed for **1P** in our earlier work.[12] The similar value of C_e can be attributed to the close chemical relationship between both molecules. The lower value of C_e can be attributed to the fact that **AP**, lacking a hydrophobic domain, does not insert as deeply as **1P** into the membrane, leaving the ester moiety more accessible to attack from water molecules.

Next, we measured the hydrolysis rate for **AP** confined inside vesicles not subjected to osmotic shock (*i.e.*, spherical unilamellar vesicles, Fig. 2(c) and Table 1). First, for the largest vesicles tested ($r = 150$ nm), the rate of hydrolysis is reduced in relation to that on the bulk, with a confinement effect on hydrolysis, C_e, on the order of 2 to 3 (Table 1, sample S1). As the size is decreased down to 75 nm, the confinement effect increases (up to 4.9 depending on the lipid composition (Table 1, sample S3)), consistent with the expected inverse relationship of C_e and vesicle radius (Fig. 1). Unexpectedly, however, when the radius of the vesicle is further reduced down to 30 nm the confinement effect slightly decreases rather than increasing (Table 1, samples S4 and S5). This outcome may be the result of a lower stability of very small vesicles and the concomitant increased leakage of the contents as the radius of the vesicle decreases. Fluorescence quenching experiments show however that there is no significant increase in the non-confined fraction of AP during the lifetime of the experiments (see ESI† Fig. S3(e) and (f)). Additionally, the fact that the apparent pH in the vesicle cavity (according to the analysis of the UV spectrum of the released pyranine) does not change during the course of the experiment is consistent with the pyranine remaining trapped within the vesicles during this time period (see the ESI, Section 2.7 and ESI Fig. S4†). Taken as a whole, these data allow us to rule out leakage as an important factor in the hydrolysis rate.

It has been shown that the affinity of a variety of biomolecules (from small peptides such as α-sinuclein to BAR domains) is dependent on the curvature of the membrane, a phenomenon that has been attributed to the presence of membrane packing defects at the level of the polar head group in curved (convex) membranes.[14–18,33] Membrane curvature and packing are intimately linked through the lipid packing parameter P.[34] Lipids with $P = 1$ have a uniform cross-sectional area, from the tail to the polar head, and for these lipids the packing is optimal when the membrane is flat (*i.e.* curvature = 0). For lipids with $P < 1$, the area of the head is larger than that of the tails, and the packing is more efficient in membranes that are convex (curvature > 0). For $P > 1$, the head has a smaller area than that of the tails and the corresponding lipids will pack more efficiently when the membrane is concave (curvature < 0). The P value for DOPC has been estimated to be 1.1.[35] The implications are that convex, flat or slightly concave membranes composed of DOPC will feature packing defects, and the number and size of these defects will decrease as a more concave curvature brings closer the head groups of the lipids (Fig. 2(d)). It is possible to estimate the packing defects of membranes using sophisticated molecular dynamics methods.[36] These are however outside the scope of the present work. For our purposes we use a simple geometric model that assumes that the presence and number of packing defects are the result of the mismatch between the packing parameter P of the lipid and the curvature of the membrane in which the lipid sits. P has been defined as the ratio between the product of the hydrophobic length and the hydrophobic volume over the area of the lipid polar head.[34] It can therefore be approximated as the ratio between the area at the hydrophobic tail end (a_m, Fig. 3(a)) and the area of the polar head (a_i, Fig. 3(a)):

$$P = \frac{a_m}{a_i} \quad (6)$$

a_m and a_i refer to the relative areas that the corresponding part of the molecule occupies under conditions of optimal membrane packing. However, as the curvature changes, the area available for each part of the molecule also changes. s_m and s_i are the total surface available at the mid-membrane and inner surface of a curved membrane (Fig. 3(a)). The optimal packing parameter of a lipid within the curved membrane is P_M:

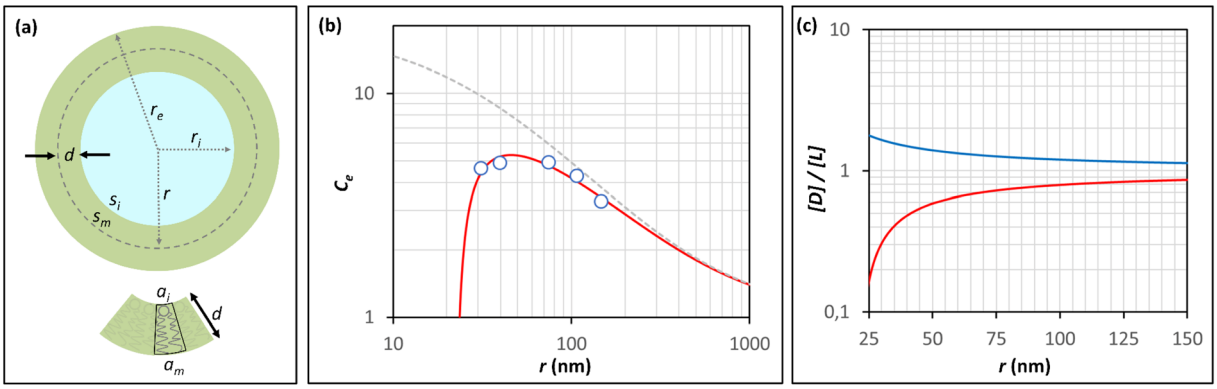

Fig. 3 Modeling the confinement effect as a function of the radius of the vesicle and the membrane packing. (a) Representation of a unilamellar spherical vesicle highlighting the geometric parameters used in the calculations. The geometric parameters of a lipid molecule sitting in the inner leaflet of the membrane are also shown. (b) Changes in the C_e for **AP** confined in lipid vesicles composed of DOPC containing 10% of DODAB with the radius of the vesicle, calculated from the hydrolysis experiments (empty circles, see Table 1 for numerical values). The red trace is the best fit to the C_e model that takes into account changes in the membrane packing with the radius, recapitulated by eqn (11). The grey dashed trace represents the theoretical changes of C_e in the absence of a membrane packing effect on **AP** binding to the membrane (*e.g.*, according to Eqn (5)). (c) Changes in the ratio between the concentration of defects, [*D*], and the concentration of lipid molecules, [*L*] with the radius of a spherical vesicle. The red trace represents the changes in concentration inside the vesicle cavity (*i.e.*, concave curvature) and the blue traces the changes in concentration in the external solution (*i.e.*, convex curvature) calculated using eqn (9) for a lipid packing parameter $P = 1.18$.

$$P_M = \frac{s_m}{s_i} \tag{7}$$

(Fig. 3(a)). Assuming a_m and a_i to remain constant, the maximum fraction of defects over the total surface, x_d, is due to the mismatch between the area covered by the lipid head groups and that of the internal surface, and can be written as a function of the packing parameters as follows:

$$x_d = 1 - \frac{P_M}{P} \tag{8}$$

For simplicity of calculations, we assume that the number of defects equals that of lipid molecules and also normalize x_d, so that it has a value of 1 when the membrane is flat. The concentration of defects displayed in the cavity of the membrane, [*D*], available for binding by the confined probe, can be written as a function of the packing parameter *P*, the half-membrane thickness *d*, and the radius of the vesicle *r* as (Fig. 3(a), see Section 3.2 of the ESI† for derivation details):

$$[D] = \frac{3P}{n_A a_m (P-1) r} - \frac{3r}{n_A a_m (r-d)^2 (P-1)} \tag{9}$$

Assuming that **AP** binds to the defects in the membrane (Fig. 2(b) and (d)), the dissociation of **AP** from the membrane defect can be written as:

$$K_d = \frac{[D][AP]}{[AP \cdot D]} \tag{10}$$

Combining eqn (1), (9) and (10) with the corresponding mass balances we can write the confinement effect as a function of all the relevant parameters, leaving the vesicle radius *r* as the only independent variable, that is (see the ESI,† Section 3.2, for the full model):

$$C_e = f(P, n_A, a_m, d, k_b, k_m, k_d, r) \tag{11}$$

For each of the membrane compositions, the experimentally determined C_e was fitted to this model. Most of the parameters were entered as known constants. Other than Avogadro's number these include a_m (0, 67 nm^2 mol^{-1})[37] and *d* (1.85 nm),[38] obtained from literature sources, and k_b and k_m, determined from the analysis of the hydrolysis of non-confined **AP** and **AP** confined in osmotically shrunk vesicles respectively. K_d and *P* were allowed to optimize during the fitting procedure. For K_d, the titration method allowed us to obtain an approximate value for vesicles with 10% DODAB only. It was therefore judged necessary to allow K_d to be optimized for all membrane compositions. For *P*, there is no agreed upon value for DOPC (the main component of our membrane in all cases) in literature sources, although it is often assumed to be slightly larger than 1.[35]

The fitting of the data to the model is remarkably good for all the experimental conditions tested (Fig. 3(b), ESI Fig. S6†). The values of K_d derived using the model range from 13 to 30 mM,

Table 2 K_d and *P* values[a]

Membrane composition	K_d (mM)	*P*
0% DODAB	27	1.16
2.5% DODAB	29	1.18
5% DODAB	31	1.19
10% DODAB	13	1.17

[a] The error of the parameters, measured as standard deviation from the fitting of the data, is on the order of 20%.

reasonably close to the titration-derived values. The values of the packing parameter P obtained range from 1.16 to 1.19, close to values of P found in literature sources.[35] These results lend support to the hypothesis that membrane packing is a key factor in modulating the chemistry inside small vesicles.

The value of P obtained does not show any discernible trend as the percentage of DODAB in the membrane increases (Table 2). This result can be attributed to the packing parameter P of DODAB being similar to that of DOPC[39] and the relatively low percentage of DODAB in relation to DOPC, combined with lack of sensitivity of the experimental method.

The difference in behavior of the C_e observed between the vesicles that have undergone osmotic shock and those that have not is consistent with the role attributed to the packing defects in the binding of **AP** to the membrane. Thus, while inside spherical vesicles **AP** is exposed to a concave membrane where the prevalence of packing defects decreases with the radius, **AP** inside osmotically shrunk vesicles is exposed to both concave and convex membranes, the latter displaying a larger amount of defects than those shown on a flat membrane. Therefore, the binding of **AP** to the membrane and the resulting C_e are not affected by the packing defect-sealing process for these vesicles.

In contrast to what takes place in the inner leaflet of the vesicle, lipid packing defects on the convex outer leaflet should increase, rather than decrease, as the vesicle radius is reduced. Therefore, the influence of the packing on the binding and the protection against hydrolysis could, in principle, also be probed by exposing non-confined **AP** to vesicles of different curvatures. However, we could not detect any meaningful difference in the binding of **AP** to the membranes when vesicles of different sizes were used (150 or 40 nm radius). This result can be attributed to both the low intrinsic affinity of **1AP** for the lipids and the lower sensitivity of packing defects' variation with the vesicle radius on the outer leaflet (Fig. 3(c)).

Concluding remarks

In this work we have shown that hydrolysis reactions are modulated by confinement within small lipid vesicles, even when the substrate is a very hydrophilic molecule. The modulation, that we term confinement effect C_e, is rooted on the binding of the substrate to the inner part of the membrane, where the hydrolysis is suppressed in relation to the hydrolysis in the bulk solution. We have shown that the extent of the modulation depends not only on the surface to volume ratio of the cavity (*i.e.*, the apparent lipid concentration in the cavity), but also on the curvature of the membrane. We attribute this observation to the progressive sealing of membrane packing defects in the concave, inner leaflet of the membrane as the radius of the vesicle decreases. The role of membrane curvature and the concomitant packing defects in regulating the binding of biomolecules has been described in the literature. However, to the best of our knowledge, this work presents the first experimental evidence in which changes in concave membrane curvature are seen to play a role in regulating the binding and, ultimately, the reactivity of molecules that are exposed to it. This conclusion is reinforced by the observation that the C_e in osmotically shrunk vesicles is much larger than in very small spherical vesicles. In osmotically shrunk vesicles, the confined probe is exposed to both concave (featuring reduced membrane packing defects) and convex (featuring slightly increased membrane packing defects) membranes, according to Cryo-EM imaging and geometric considerations. Additional evidence of the validity of this conclusion was obtained by fitting the changes observed in C_e with the radius of the vesicle to a mathematical model which assumes that C_e depends not only on the binding affinity of the probe for the membrane, but also on the lipid packing parameter. The fitting of the data is excellent and the value of the packing parameter obtained from the fitting is remarkably close to the literature values for the main lipid used (DOPC). It cannot be discarded that changes in fluidity, or structural changes other than packing defects in a highly concave membrane play a role in the phenomenon observed. In order to elucidate this point, we are currently developing a computational method to model membranes of different curvatures, whose predictions will be contrasted with experimental data using lipids with different packing parameters. The results will allow us to refine the model, incorporating the contribution of all relevant phenomena. In summary, this work illustrates that chemical reactivity in membrane bound compartments is modulated by the membrane and its structure, provided that the ratio of surface to volume is large enough. Thus, within living cells, the background (*i.e.*, non-enzyme catalyzed) reactions of small molecules will depend on whether they are found trapped within small, spherical transport vesicles, or in non-spherical compartments, such as the endoplasmic reticulum or the Golgi apparatus. It is also reasonable to expect that the extent of membrane binding of confined enzymes will be different, which may modulate enzyme activity according to the shape of the compartment. In the field of nano-reactors and vesicle-based drug delivery vehicles, these results and the mathematical treatment we propose offer useful tools for the design of vesicles with predictable reaction rates of the confined molecules. The results also show that a stimulus that changes the affinity of confined molecules for the membrane (here osmotic shock) may modulate its reactivity. Since the membrane is in direct contact with, and responds to, changes in the environment, these processes can be seen as a crude form of signal transduction where the membrane as a whole acts as the transducer. We propose that this form of transduction was present from the onset of abiogenesis and would have played a role in shaping the evolution towards protocells. While in modern cells this form of transduction is likely obscured by very efficient and complex biomolecular machinery, understanding its potential will allow devising comparatively simple (and inexpensive) vesicle-based systems for bio sensing and drug delivery.

Data availability

Cryo-EM data can be found as part of the ESI.† Spectrosocpic data is avaliable from the authors upon request.

Author contributions

BW carried out all the experiments (except EM), analysed the data and wrote the manuscript (investigation, methodology, formal analysis, validation, writing-original draft and writing-review and editing). KT and NS co-supervised the research, contributed to the design of the experiments and wrote the manuscript (supervision, conceptualization, methodology, writing-review and editing), SC carried out the EM experiments and wrote the manuscript (investigation, writing-review and editing). LM designed the EM experiments and analysed the EM images and wrote the manuscript (methodology, formal analysis, writing-original draft and writing-review and editing). ST designed the experiments, supervised the research, analysed the data and wrote the manuscript (conceptualization, project administration, supervision, methodology, formal analysis, writing-original draft and writing-review and editing).

Conflicts of interest

There are no conflicts to declare.

References

1 G. V. Oshovsky, D. N. Reinhoudt and W. Verboom, *Angew. Chem., Int. Ed.*, 2007, **46**, 2366.
2 D. Vieira, K. Kleinermanns, W. F. Martin and M. Preiner, *FEBS Lett.*, 2020, **549**, 2717.
3 P. Siekevitz, *Protein Synthesis and the Ribosome*, eds Ord M. G. and Stocken L. A., Foundations of Modern Biochemistry, 1996, vol. 2, ch. 5, p. 109.
4 D. B. Cowie and B. P. Walton, *Biochim. Biophys. Acta*, 1956, **21**, 211.
5 A. Radzicka and R. Wolfenden, *J. Am. Chem. Soc.*, 1996, **118**, 6105.
6 S. Becker, C. Schneider, H. Okamura, A. Crisp, T. Amatov, M. Dejmek and T. Carell, *Nat. Commun.*, 2018, **9**, 163.
7 B. Damer and D. Deamer, *Astrobiology*, 2020, **20**, 429.
8 S. Murillo-Sanchez, D. Beaufils, J. M. G. Manas, R. Pascal and K. Ruiz-Mirazo, *Chem. Sci.*, 2016, **7**, 3406.
9 D. W. Armstrong, R. Seguin, C. J. McNeal, R. D. Macfarlane and J. H. Fendler, *J. Am. Chem. Soc.*, 1978, **100**, 4605.
10 M. Blocher, D. J. Liu, P. Walde and P. L. Luisi, *Macromolecules*, 1999, **32**, 7332.
11 K. Adamala and J. W. Szostak, *Nat. Chem.*, 2013, **5**, 495.
12 A. Grochmal, L. Prout, R. Makin-Taylor, R. Prohens and S. Tomas, *J. Am. Chem. Soc.*, 2015, **137**, 12269.
13 P. M. Frederik and M. M. H. Storms, *Microsc. Today*, 2005, **13**, 32.
14 J. B. Larsen, C. Kennard, S. L. Pedersen, K. J. Jensen, M. J. Uline, N. S. Hatzakis and D. Stamou, *Biophys. J.*, 2017, **113**, 1269.
15 N. S. Hatzakis, V. K. Bhatia, J. Larsen, K. L. Madsen, P. Y. Bolinger, A. H. Kunding, J. Castillo, U. Gether, P. Hedegard and D. Stamou, *Nat. Chem. Biol.*, 2009, **5**, 835.
16 J. Liu, B. Bu, M. Crowe, D. C. Li, J. J. Diao and B. H. Ji, *Phys. Chem. Chem. Phys.*, 2021, **23**, 2117.
17 L. Mei, W. H. Shen, X. W. Wu, J. Liu, D. C. Li and B. H. Ji, *Theor. Appl. Mech. Lett.*, 2020, **10**, 412.
18 B. J. Peter, H. M. Kent, I. G. Mills, Y. Vallis, P. J. G. Butler, P. R. Evans and H. T. McMahon, *Science*, 2004, **303**, 495.
19 S. S. Mansy, J. P. Schrum, M. Krishnamurthy, S. Tobe, D. A. Treco and J. W. Szostak, *Nature*, 2008, **454**, 122.
20 C. Bonfio, D. A. Russell, N. J. Green, A. Mariani and J. D. Sutherland, *Chem. Sci.*, 2020, **11**, 10688.
21 M. Imai, Y. Sakuma, M. Kurisu and P. Walde, *Soft Matter*, 2022, **18**, 4823.
22 I. Gozen, E. S. Koksal, I. Poldsalu, L. Xue, K. Spustova, E. Pedrueza-Villalmanzo, R. Ryskulov, F. D. Meng and A. Jesorka, *Small*, 2022, **18**, 2106624.
23 D. A. Wilson, R. J. M. Nolte and J. C. van Hest, *Nat. Chem.*, 2012, **4**, 268.
24 L. Schoonen and J. C. van Hest, *Adv. Mat.*, 2016, **28**, 1109.
25 M. J. Langton, F. Keymeulen, M. Ciaccia, N. H. Williams and C. A. Hunter, *Nat. Chem.*, 2017, **9**, 426.
26 Y. Zhong, F. Meng, W. Zhang, B. Li, J. C. M. van Hest and Z. Zhong, *J. Controlled Release*, 2020, **320**, 421.
27 M. J. Langton, L. M. Scriven, N. H. Williams and C. A. Hunter, *J. Am. Chem. Soc.*, 2017, **139**, 15768.
28 A. Joseph, C. Contini, D. Cecchin, S. Nyberg, L. Ruiz-Perez, J. Gaitzsch, G. Fullstone, X. Tian, J. Azizi, J. Preston, G. Volpe and G. Battaglia, *Sci. Adv.*, 2017, **3**(8), e1700362.
29 I. A. Chacko, V. M. Ghate, L. Dsouza and S. A. Lewis, *Colloids Surf., B*, 2020, **195**, 111262.
30 A. Müller and B. König, *Chem. Commun.*, 2014, **50**, 12665.
31 T. Ivanović, D. Z. Popović, J. Miladinović, J. A. Rard, Z. P. Miladinović and F. T. Pastor, *J. Chem. Eng. Data*, 2020, **65**, 5137.
32 K. S. Pitzer, J. C. Peiper and R. H. Busey, *J. Phys. Chem. Ref. Data*, 1984, **13**, 1.
33 J. Bigay and B. Antonny, *Dev. Cell*, 2012, **23**, 886.
34 J. N. Israelachvili, D. J. Mitchell and B. W. Ninham, *J. Chem. Soc., Faraday Trans. 2*, 1976, **72**, 1525.
35 D. Marsh, *Biophys. J.*, 1996, **70**, 2248.
36 R. Gautier, A. Bacle, M. L Tiberti, P. F. Fuchs, S. Vanni and B. Antonny, *Biophys. J.*, 2018, **115**, 436.
37 N. Kučerka, J. F. Nagle, J. N. Sachs, S. E. Feller, J. Pencer, A. Jackson and J. Katsaras, *Biophys. J.*, 2008, **95**, 2356.
38 N. Kučerka, S. Tristram-Nagle and J. F. Nagle, *J. Membr. Biol.*, 2006, **208**, 193.
39 D. F. Evans and B. W. Ninham, *J. Phys. Chem.*, 1986, **90**(2), 226.